Science in China Series B: Chemistry

www.scichina.com
chem.scichina.com
www.springerlink.com

Theoretical study on $S_1(^1B_{3u})$ state electronic structure and absorption spectrum of pyrazine

HE RongXing[1], ZHU ChaoYuan[2†], CHIN Chih-Hao[3] & LIN Sheng-Hsien[2,3]

[1] College of Chemistry and Chemical Engineering, Southwest University, Chongqing 400715, China;
[2] Department of Applied Chemistry, Institute of Molecular Science and Center for Interdisciplinary Molecular Science, National Chiao-Tung University, Hsinchu 300, China;
[3] Institute of Atomic and Molecular Sciences, Academia Sinica, Taipei 106, China

Making use of a set of quantum chemistry methods, the harmonic potential surfaces of the ground state ($S_0(^1A_g)$) and the first ($S_1(^1B_{3u})$) excited state of pyrazine are investigated, and the electronic structures of the two states are characterized. In the present study, the conventional quantum mechanical method, taking account of the Born-Oppenheimer adiabatic approximation, is adopted to simulate the absorption spectrum of $S_1(^1B_{3u})$ state of pyrazine. The assignment of main vibronic transitions is made for $S_1(^1B_{3u})$ state. It is found that the spectral profile is mainly described by the Franck-Condon progression of totally symmetric mode ν_{6a}. For the five totally symmetric modes, the present calculations show that the frequency differences between the ground and the $S_1(^1B_{3u})$ state are small. Therefore the displaced harmonic oscillator approximation along with Franck-Condon transition is used to simulate $S_1(^1B_{3u})$ absorption spectra. The distortion effect due to the so-called quadratic coupling is demonstrated to be unimportant for the absorption spectrum, except the coupling mode ν_{10a}. The calculated $S_1(^1B_{3u})$ absorption spectrum is in reasonable agreement with the experimental spectra.

pyrazine, absorption spectrum, quantum mechanical method, electronic structure

1 Introduction

The electronic structures and absorption spectra of pyrazine have attracted much attention over the past several decades as it is one of the especially significant molecules in relation to intramolecular electronic relaxation[1,2]. In the experimental studies[3−5], the absorption spectra and the electronic structures of the low-lying excited state have been determined accurately; the first excited state $S_1(^1B_{3u})$ has an $n\pi^*$ electronic configuration, and the second excited state $S_2(^1B_{2u})$ has a $\pi\pi^*$ feature. The so-called "channel three" problem well studied in the benzene has also been demonstrated in pyrazine[3]. That is, the non-radiative decay of $S_2(^1B_{2u})$ state increases sharply when the excitation energy is above a threshold, which makes the two types of lowest singlet excited state have different features of the absorption spectra.

In the aspect of the theoretical investigations, the spectroscopies and the radiationless decay dynamics of the $S_1(^1B_{3u})$ and $S_2(^1B_{2u})$ state were explored in great detail by means of several different methods[63−11]. Seidner et al. set up an S_1-S_2 vibronic-coupling model consisting of four most important vibrational modes (ν_1, ν_{6a}, ν_{9a} and ν_{10a})[6,7,12]. Most recently, Shalashilin et al.[10] reported the quantum simulation of absorption spectrum of pyrazine based on the coupled coherent state (CCS)[13] technique. In the previous theoretical studies, the absorption spectra of pyrazine were calcu-

Received May 30, 2008; accepted July 8, 2008
doi: 10.1007/s11426-008-0124-2
†Corresponding author (email: cyzhu@mail.nctu.edu.tw)
Supported by Taiwan National Science Council (Grant Nos. NSC 96-2113-M-009-021 and NSC 96-2811-M- 009-023)

lated by considering the vibronic coupling of $S_1(^1B_{3u})$ and $S_2(^1B_{2u})$ state. As demonstrated in the previous studies, the vibrational mode ν_{10a}, the single normal mode of pyrazine which can couple the $S_1(^1B_{3u})$ and $S_2(^1B_{2u})$ state in the first order, plays an important role in the simulation of absorption spectra. However, it is not really well understood that how this vibronic coupling affects absorption spectra in detail, namely, what could happen if this coupling is not included in the simulation. This is one of the questions the present study wants to answer. In the present work, the general quantum mechanic method without considering the conical intersection of $S_1(^1B_{3u})$ and $S_2(^1B_{2u})$ state is performed to characterize the $S_1(^1B_{3u})$ absorption spectrum of pyrazine. In this method, the Born-Oppenheimer and harmonic approximations are adopted. The predicted absorption band shape is compared with experimental spectrum. It is known that the vibrational modes of molecules are defined with respect to the potential energy surface minimum and are described well by harmonic oscillators near the equilibrium position. The geometries of the ground and first excited state are required in order to calculate the absorption coefficient in the present theory. Therefore, another goal of the present study will be to perform the characterizations of geometries and electronic structures of the ground state and the first excited state.

2 Method and theory

2.1 Computational methods

The geometries of the ground state ($S_0(^1A_g)$)of pyrazine in vapors is optimized at MP2 level with 6-311++G** basis set. Then, the optimization of $S_0(^1A_g)$ is carried out again using the multi-reference CASSCF approach with the same basis set in terms of that the first low-lying excited state $S_1(^1B_{3u})$ is optimized. For comparison, the ground state is optimized with the HF method and the first excited stated is optimized with CIS method with the same 6-311++G** basis set. The active space used in CASSCF calculations of the two electronic states consists of eight active orbitals and ten active electrons (denoted as (10e, 8o)), that is, ten electrons are distributed in six valence orbitals (three of which are occupied and three are unoccupied) and two occupied nonbonding orbitals located on nitrogen. This kind of selection of the active space is demonstrated by Woywood et al.[8] to be appropriate. The stability of all the optimized geometries is checked by the frequency simulation in which the normal modes and the harmonic vibrational frequencies of pyrazine in the two electronic states are all obtained. The Gaussian03 program package[14] is used for all the above-mentioned calculations.

As the time-dependent density functional theory (TDDFT) is now available for excited-state geometry optimization[15]. It is very interesting to see if the geometry of excited state $S_1(^1B_{3u})$ is also optimized by means of the hybrid functional BHLYP with aug-cc-pVDZ basis set, and then the simulated results are compared with the CIS and CASSCF results. The TDDFT calculation is carried out by the TURBOMOLE 5.9 package[16].

2.2 General theory

In this section, the basic theoretical approach used in the calculations of spectra is presented briefly. In gas phase, the absorption coefficient $\alpha(\omega)$ for the electronic transition from state a to state b with vibrational quanta v and v', respectively, can be expressed as[17,18]

$$\alpha(\omega) = \frac{4\pi^2\omega}{3\hbar c} \cdot \left|\vec{\mu}_{ba}\right|^2 \sum_{v}\sum_{v'} P_{av} \left|\langle \Theta_{bv'} | \Theta_{av} \rangle\right|^2 D(\omega_{bv',av} - \omega), \quad (1)$$

in which the Born-Oppenheimer adiabatic approximation is used, $\left|\langle \Theta_{bv'} | \Theta_{av} \rangle\right|^2$ represents the Franck-Condon factor, $\left|\vec{\mu}_{ba}\right|^2$ denotes the electronic transition dipole moment, P_{av} the Boltzmann factor, c the speed of light and $D(\omega_{bv',av} - \omega)$ the Lorentzian line-shape function. As shown in the previous theoretical calculations[6,7] within the harmonic approximation, the wave function of system is assumed to be that of harmonic oscillator and can be expressed as a product of wave function of each mode,

$$\Theta_{av} = \prod_i \chi_{av_i}(Q_i), \quad \Theta_{bv'} = \prod_i \chi_{bv'_i}(Q'_i), \quad (2)$$

where $\chi_{av_i}(Q_i)$ and $\chi_{bv'_i}(Q'_i)$ represent the vibrational wave functions belonging to electronic state a and b, respectively. For an allowed transition with the harmonic surfaces, Eq. (1) can be rewritten as

$$\alpha(\omega) = \frac{2\pi\omega}{3\hbar c}\left|\vec{\mu}_{ba}\right|^2 \int_{-\infty}^{\infty} \mathrm{d}t \exp(\omega_{ba} - \omega) \prod_i G_i(t), \quad (3)$$

and

$$G_i(t) = \sum_{v_i}\sum_{v_i'} P_{av_i} \left| \left\langle \chi_{bv_i'} \middle| \chi_{av_i} \right\rangle \right|^2 \times \exp\left\{ it\left[\left(v_i' + \frac{1}{2} \right)\omega_i' - \left(v_i + \frac{1}{2} \right)\omega_i \right] \right\}. \quad (4)$$

Here, ω_i and ω_i' are the oscillator frequencies of the ith mode in the electronic state a and b, and ω_{ba} denotes the electronic energy gap. Using the relation of the Slater sum[19], we have

$$G_i(t) = 2\sqrt{\beta_i\beta_i'} \sinh(\hbar\omega_i / 2kT) \times \exp\left[-\beta_i\beta_i' d_i^2 \tanh(\lambda_i/2)\tanh(\mu'/2) / \left(\beta_i \tanh(\lambda_i/2) + \beta_i' \tanh(\mu'/2) \right) \right] / \left[\sinh\lambda_i \sinh\mu_i' \left(\beta_i \tanh(\lambda_i/2) + \beta_i' \tanh(\mu'/2) \right) \cdot \left((\beta_i \coth(\lambda_i/2) + \beta_i' \coth(\mu'/2) \right) \right]^{1/2}, \quad (5)$$

where

$$\beta_i = \frac{\omega_i}{\hbar},\ \lambda_i = \frac{\hbar\omega_i}{kT} + it\omega_i,\ \mu_i' = -it\omega_i',\ d_i = Q_i' - Q_i, \quad (6)$$

in which d_i denotes the normal coordinate difference of the two electronic states. For the displaced oscillators, $\beta_i = \beta_i'$ and $d_i \neq 0$, then Eq. (3) is deduced to

$$\alpha(\omega) = \frac{2\pi\omega}{3\hbar c} \left| \vec{\mu}_{ba} \right|^2 \int_{-\infty}^{\infty} dt \exp \left[it(\omega_{ba} - \omega) - \gamma_{ba}|t| - \sum_i S_i \left\{ (2\bar{n}_i + 1) - (\bar{n}_i + 1)e^{it\omega_i} - \bar{n}_i e^{-it\omega_i} \right\} \right], \quad (7)$$

where γ_{ba} represents the dephasing (or damping) constant, which is related to the lifetime and pure dephasing of the two states; $\bar{n}_i = (e^{\hbar\omega_i/kT} - 1)^{-1}$, the phonon distribution; S_i denotes the Huang-Rhys factor, which can be written as,

$$S_i = \frac{\omega_i}{2\hbar} d_i^2. \quad (8)$$

The absorption coefficient can be calculated using Eq. (7) and then the spectra are simulated.

3 Results and discussion

3.1 Geometries of $S_0(^1A_g)$ and $S_1(^1B_{3u})$ state

The geometrical parameters of pyrazine in its electronic ground state and the first excited state are shown in Table 1, together with the experimental[4] and the other available theoretical data[7,20]. In the present study, the MP2, CASSCF, HF and hybrid functional BHLYP are utilized to optimize the equilibrium geometry of ground state, and the CASSCF, CIS and TD-BHLYP are used to optimize the equilibrium geometry of the excited state. As Seidner[7] and Raab[9] demonstrated, for the $S_0(^1A_g)$ surface in the vicinity of the equilibrium geometry, MP2 method can provide rather accurate geometry parameters and vibrational frequencies (Table 2) . By the inspection of Tables 1 and 2, we show that our MP2 results are indeed in good agreement with the previous computational and experimental data. Actually, the present CASSCF results in Tables 1 and 2 also show accurate geometry for the ground state.

The simulated results for the first excited state, $S_1(^1B_{3u})$, are shown in Table 1, showing that all the CC bonds and CN bonds of $S_1(^1B_{3u})$ state are longer compared with those of the ground state, that is, the molecu-

Table 1 The selected geometrical parameters of $S_0(^1A_g)$ and $S_1(^1B_{3u})$ state obtained in the present work[a)] and the experimental[b)] and previous theoretical data[c), d)]

		CC	CN	CH	∠NCC	∠CNC	∠NCH	∠CCNC
$S_0(^1A_g)$	MP2	1.399 (1.403)	1.344 (1.339)	1.087 (1.115)	122.4 (122.2)	115.1 (115.6)	116.9 (113.9)	0.0 (0.0)
	CASSCF	1.395	1.329	1.075	122.0	116.1	117.2	0.0
	BHLYP	1.390	1.325	1.084	121.9	116.3	117.4	0.0
	HF	1.387	1.317	1.075	121.7	116.6	117.5	0.0
	Calc. c)	1.402	1.346	1.085	122.3	115.3	116.8	
$S_1(^1B_{3u})$	CASSCF	1.431	1.369	1.074	124.0	112.1	116.8	0.0
	BHLYP	1.391	1.334	1.082	119.8	120.3	121.1	0.0
	CIS	1.388	1.328	1.074	119.7	120.7	120.9	0.0
	Calc. d)	1.395	1.352	1.086		118.4	119.7	

a) The used basis set is aug-cc-pVDZ for functional BHLYP by Turbomole code, and 6-311++G** for other theoretical levels by Gaussian03 program; the experimental data are given in parentheses. The bond lengths are in angstrom and the angles in degree; b) ref.[4]; c) ref.[7]; d) ref.[20].

Table 2 The Huang-Rhys factors and vibrational frequencies (cm^{-1}) of the five totally symmetric modes and the coupling mode

Sym	mode	$S_0(^1A_g)$						$S_1(^1B_{3u})$								
		Expt.[a)]	Calt.[b)]	MP2	CAS	BHLYP	HF	Expt.[c)]	CAS	BHLYP	CIS	S [d)]	S [e)]	S [f)]	κ_i [g)]	S [h)]
A_g	ν_{6a}	596	597	601	643	608	655	585	568	629	660	0.420	0.087	0.116	–0.0964	0.837
	ν_1	1015	1027	1027	1074	1038	1118	970	988	1085	1090	0.245	0.016	0.028	–0.0470	0.068
	ν_{9a}	1230	1264	1258	1324	1244	1647	1104	1303	1291	1283	0.029	0.251	0.204	0.1594	0.526
	ν_{8a}	1582	1633	1613	1730	1615	1789	1377	1674	1706	1667	0.091	0.904	0.700	–0.0623	0.049
	ν_2	3055	3280	3221	3352	3177	3354		3287	3311	3372	0.028	0.099	0.113	0.0368	0.004
B_{1g}	ν_{10a}	919	914	903	953	984	1034	383	682	443	324	0.000	0.000	0.000		

a) Ref.[4]; b) refs.[7,9]. The optimization was performed at MP2/DZP level; c) ref.[5]; d) The CASSCF Huang-Rhys factors. These values are calculated using the frequencies obtained by MP2 and the geometries optimized by CASSCF; e) The BHLYP Huang-Rhys factors. Turbomole code is performed; f) The CIS Huang-Rhys factors. The geometry of $S_0(^1A_g)$ state is optimized at HF level, and that of $S_1(^1B_{3u})$ state is optimized at CIS level; g) The gradients of the excitation energy with respect to the totally symmetric normal coordinates (data are from ref. [8]). These data were calculated by MRCI method. Units are in eV; h) The corresponding Huang-Rhys factors from gradients.

lar ring is expanded. For example, the CC bond of $S_0(^1A_g)$ calculated by CASSCF is 1.395 Å, but that of $S_1(^1B_{3u})$ from the same level is 1.431 Å. This result is understandable due to the electronic transition in the first excited state. It is well known that the $S_1(^1B_{3u})$ is an nπ* state, indicating that an n-type electron located on nitrogen atom is transferred to the antibonding π* orbital on the pyrazine ring when excitation takes place. This leads to the longer bonds due to the increase of charge located on the antibonding orbital. According to our calculations, it is predicted that the first excited state results mainly from the excitation from HOMO orbital to LUMO orbital. Obviously, HOMO is an n-type orbital and LUMO is a π-type one (Figure 1), which confirms the nπ* feature of $S_1(^1B_{3u})$ state. Because of the same level of theory, CIS data are compared with those of HF. As can be seen from Table 1, the CC bonds and CN bonds of CIS are also elongated slightly with respect to that of HF, indicating that CIS is also able to give an acceptable optimized geometry of the first excited state.

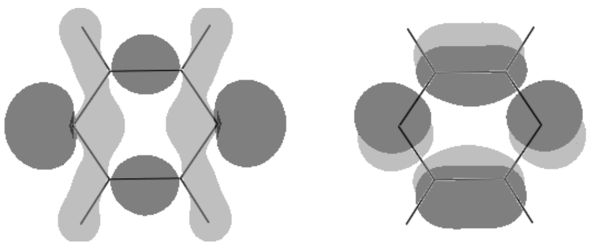

Figure 1 The frontier molecular orbitals involved in the low-lying excited state.

Further, it is found that the TD-BHLYP results are closer to CIS ones.

As shown in Table 2, for the ground state of pyrazine, MP2 provides very accurate harmonic vibrational frequencies (only the five totally symmetric modes ν_1, ν_2, ν_{6a}, ν_{8a} and ν_{9a} and coupling mode ν_{10a} are listed). One can see that the frequencies of CASSCF and HF are overestimated slightly relative to those of MP2 and functional BHLYP. For the two types of electronic state $S_0(^1A_g)$ and $S_1(^1B_{3u})$, the harmonic frequencies predicted by CASSCF are nearly identical, and they agree with the MP2 frequencies very well for $S_0(^1A_g)$ state. For the mode $\nu_{6\alpha}$, for example, the CASSCF frequencies of $S_0(^1A_g)$ and $S_1(^1B_{3u})$ state are 643 and 568 cm^{-1}, which have a small difference with respect to the MP2 one, 601 cm^{-1} for $S_0(^1A_g)$ state. This indicates that the displaced harmonic oscillator approximation is reasonable. However, for the BHLYP results, it is noted that the ground-state frequencies of modes ν_{6a} and ν_1 are larger than the excited-state ones, which is different from other theoretical data.

3.2 Excitation energy and absorption spectrum

Given in Table 3 are the vertical excitation energy (ΔE), transition dipole moments and oscillator strengths (*f*) of the $S_1(^1B_{3u})$ state. Compared with experiment, it is found that the CIS nπ* transition energy is about 0.94 eV, that is, CIS significantly overestimates the excitation energy. Eq. (9) is often used to correct the CIS transition energy[21]:

Table 3 The calculated vertical excitation energy, transition dipole moments and oscillator strengths[a)], together with the experimental and previous theoretical data

	CIS	TD-B3LYP	TD-BHLYP	CASSCF [c)]	Calc. [d)]	Expt. [e)]
$\Delta E(S_1, n\pi^*)$	4.88(3.98) [b)]	3.94	4.40	3.73	4.65	3.94
μ_{10}	0.274	0.241	0.273			
f_{10}	0.009	0.006	0.006		0.010	0.006

a) In this work, basis set aug-cc-pVDZ is used for TD-BHLYP and 6-311++G** is used for other theoretical levels; b) the energy in parentheses is corrected using eq. (9); c) the energy is corrected using MP2 method; d) ref. [8]. The calculations were performed at MRCI/DZP level considering the state average; e) ref. [4].

$$E_{\exp t.} = 1.02E_{calc.} - 1.00\,(\mathrm{e}V)\,. \tag{9}$$

From Table 3, we can see the corrected excitation energy is acceptable. In addition, the TDDFT gives reliable excitation energy for low-lying state in which the functional B3LYP is chosen to estimate the vertical transition energy of nπ* state. Apparently, the TD-B3LYP level provides an appropriate vertical excitation energy for the nπ* state. Most recently, Li et al.[22] reported the excitation energy of pyrazine using B3LYP method, and the results are consistent with our present calculations. However, the excitation energy calculated by TD-BHLYP/aug-cc-pVDZ is greater in comparison with the experimental data. In order to obtain more reasonable excitation energy, MP2 correction based on the CASSCF geometry is performed, and the experimental vertical excitation energy of $S_1(^1B_{3u})$ state is satisfactorily reproduced by our calculations.

In this section, the absorption spectra of $S_1(^1B_{3u})$ state of pyrazine will be detected by the method described in section Ⅱ B. As shown in Table 3, the predicted vertical excitation energy, which determines the exact position of the absorption band in the absolute energy scale, is slightly different from the experimental data. For the purpose to make the absorption spectra have correct position to conveniently compare with the experimental bands, the vertical excitation energy is adjusted to obtain the same value as the experimental data. This strategy was adopted by the previous literature[7,8]. In addition, the MP2 frequencies will be used to calculate the Huang-Rhys factor (S_i) due to the excellent agreement with the experimental data. Using Eq. (8), the Huang-Rhys factors of the first excited singlet state of pyrazine are calculated and the results are listed in Table 2. The temperature 298 K is taken in the theoretical calculations (the experimental spectra were obtained at room temperature)[3].

The Huang-Rhys factors (S_i, i denote the normal modes) of the five Franck-Condon active totally symmetric normal modes and the coupling mode ν_{10a} are shown in Table 2 (S_i of non-totally symmetric normal modes are zero). For CASSCF results, the largest factor, S_{6a}, is less than 1.0 (0.420). This indicates that the probability of the 0-0 transition is the highest when electron excitation takes place. Figure 2(a) shows the experimental gas-phase absorption spectrum of $S_1(^1B_{3u})$ state of pyrazine[3]. A striking feature is that there are two strong peaks, and the stronger band is assigned as 0-0 transition. Figure 2(b) displays that the simulated absorption spectrum after convolution of the calculated stick spectrum with a Lorentzian broadening (the normal coordinate difference of $S_0(^1A_g)$ and $S_1(^1B_{3u})$ state, d_i, is calculated by CASSCF). The Lorentzian width of each transition is assumed to be proportional to the vibrational energy and about 500 fs is taken for the dephasing constant γ_{ba}. It seems that the calculated $S_1(^1B_{3u})$ absorption spectrum in this work only reproduces qualitatively the essential features in comparison with the experimental observation. We present the tentative assignment of vibrational transition in the absorption spectrum of $S_1(^1B_{3u})$ state. Obviously, the spectral profile is mainly described by the Franck-Condon progression of mode ν_{6a}, which is in good agreement with the experimental assignments[3−5]. The intensity of the vibronic line assigned as $6a^1$, however, is somewhat underestimated in the present calculation. Table 2 shows that in the experimental data, the frequency difference between $S_0(^1A_g)$ and $S_1(^1B_{3u})$ state for coupling mode ν_{10a} is large (the frequency is 919 cm^{-1} for S_0 state and 383 cm^{-1} for S_1 state). This means that the distorted effect of mode ν_{10a} is significant for the $S_1(^1B_{3u})$ spectrum (see Section 3.3, the distorted effect is estimated by Eq. (10)). For simplicity, only the vibronic lines $10a^2$ are calculated and the result is shown in Figure 2(b). In addition, the vibronic line $10a^1$ induced by the mode ν_{10a} was not re-

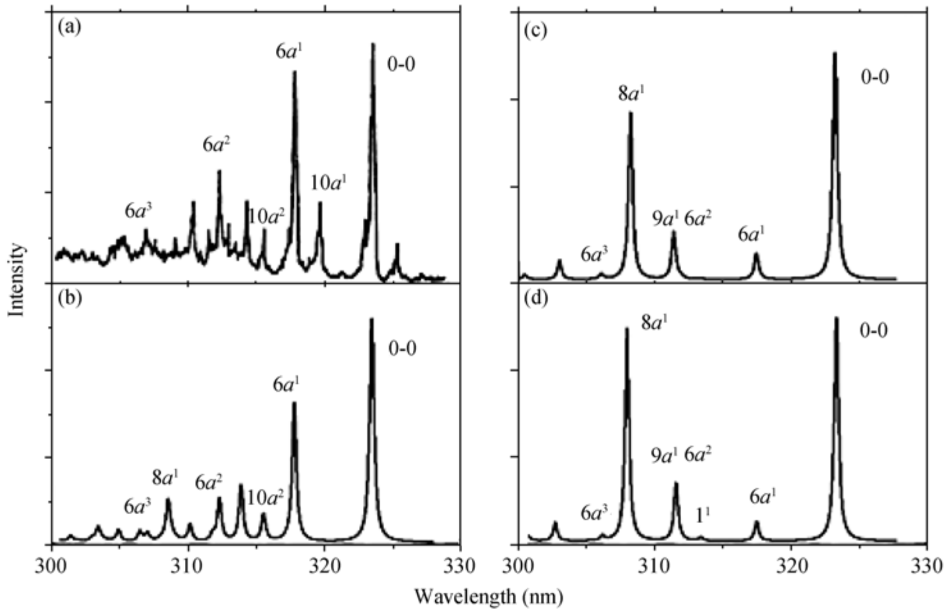

Figure 2 The $S_1(^1B_{3u})\leftarrow S_0(^1A_g)$ absorption spectrum of pyrazine. (a) The experimental spectrum (ref. [3]); (b) the calculated spectrum by CASSCF; (c) by CIS; (d) by BHLYP.

produced correctly in our work due to the Huang-Rhys factor of this mode being almost zero. This can be attributed to the effect of vibronic coupling between $S_2(^1B_{2u})$ and $S_1(^1B_{3u})$ state that is not taken into account in this work, which will be reported in a future paper.

The similar calculations are carried out to simulate the $S_1(^1B_{3u})$ absorption spectrum by means of the CIS and BHLYP geometries, and the results are shown in Figure 2(c) and (d), respectively. Compared with the CASSCF spectrum, the CIS and BHLYP methods present a large inconsistency between calculated and experimental results, which suggests the geometry of $S_1(^1B_{3u})$ state optimized by CIS and BHLYP might be unreasonable. As shown in Figure 2, an unexpected thing is that the simulated absorption spectra of $S_1(^1B_{3u})$ state by CIS and BHLYP are almost identical. The Huang-Rhys factors by these two methods are shown in Table 2. Obviously, the totally symmetric mode ν_{8a} has the largest Huang-Rhys factor for the two methods (0.700 for CIS and 0.775 for BHLYP), which leads to the conflicting $S_1(^1B_{3u})$ spectrum.

3.3 Discussion

The absorption spectra of $S_1(^1B_{3u})$ state in pyrazine are simulated by employing the conventional methods[18], in which the Born-Oppenheimer adiabatic approximation and displaced oscillator approximation are used. In the displaced oscillator approximation, the Franck-Condon factor can be expressed as

$$F_{v_i'} = \frac{S_i^{v_i'}}{v_i'!} e^{-S_i}, \tag{10}$$

where v_i' denotes the vibrational quantum number of ith normal mode, and S_i is the Huang-Rhys factor. When S_i =0, Eq. (10) is zero, so that we have to consider correction to Franck-Condon factor from the distorted oscillator approximation,

$$F_{v_i'} = \frac{\sqrt{\omega_i \omega_i'}}{\omega_i + \omega_i'} \left(\frac{\omega_i' - \omega_i}{\omega_i' + \omega_i} \right)^{v_i'} \frac{v_i'!}{2^{v_i'-1} \left[(v_i'/2)! \right]^2}, \tag{11}$$

where v_i' is an even integer. We can see that unless $\omega_i' >> \omega_i$ (or $\omega_i' << \omega_i$), $F_{v_i'}$ is much smaller than unity in most cases. In other words, the distortion effect due to the so-called quadratic coupling is unimportant. For example, for the ν_4 mode in CASSCF calculations (the frequencies are not shown in Table 2), $\omega_4(S_0) = 777\ \text{cm}^{-1}$, while $\omega_4(S_1) = 491\ \text{cm}^{-1}$ (Table 2), and $F_{2'_{6b}} / F_{0'_{6b}}$ in this case is only 0.025. This value is too small to affect the $S_1(^1B_{3u})$ spectral profile. However, the frequency difference between S_0 and S_1 state for mode ν_{10a} is large (other modes are very small), that is, the distorted effect of mode ν_{10a} is not negligible, and in this way, we estimate this distorted contribution and plot it in Figure 2(b). It should be emphasized that the distorted correction in Eq. (11) is attributed to that vibrational quantum number v_i' is even integer. That means the vibronic lines 10a^2, 10a^4, ..., are due to distorted contributions, but the lines 10a^1, 10a^3, …, are not.

The present model without considering conical intersection is the same as the previous theoretical model in nature[6−8]. Taking the *ab initio* data from ref. [8], the absorption spectra of $S_1(^1B_{3u})$ state of pyrazine can be calculated by means of Eq. (3) or Eq. (7). According to the model proposed by Woywood et al.[8], the excited state Hamiltonians can be expressed as

$$H_k = \sum_i \frac{\omega_i}{2}\left(-\frac{\partial^2}{\partial Q_i^2} + Q_i^2\right) + E_k + \sum_i \kappa_i^{(k)} Q_i + \sum_{i,j} \gamma_{i,j}^{(k)} Q_i Q_j, \quad (12)$$

where ω and Q represent the vibrational frequencies and coordinates, respectively; k=1, 2, denotes the excited state $S_1(^1B_{3u})$ and $S_2(^1B_{2u})$; *i, j* include the totally symmetric modes (ν_1, ν_{6a}, ν_{9a}, ν_{8a},ν_2) and the S_1-S_2 coupling mode ν_{10a}; $\gamma_{i,j}^{(k)}$ for $i \neq j$ is responsible for the Duschinsky effect and $\gamma_{i,i}^{(k)}$ is responsible for the normal mode frequency modifications. In the present work, $\gamma_{i,j}^{(k)}$ are neglected due to their small values[8], and all five totally symmetric modes are considered to be Franck-Condon active. In this case, Eq. (12) can be written as

$$H_k = \sum_i \frac{\omega_i}{2}\left(-\frac{\partial^2}{\partial Q_i^2} + Q_i^2\right) + E_k + \sum_i \kappa_i^{(k)} Q_i, \quad (13)$$
$$(i = \nu_1,\ \nu_2, \nu_{6a},\ \nu_{8a}, \nu_{9a})$$

where $\kappa_i^{(k)}$ denotes the gradients of the excitation energy E_k (k=1, 2) of $S_1(^1B_{3u})$ and $S_2(^1B_{2u})$ state with respect to the totally symmetric coordinates. In order to calculate the Huang-Rhys factors, we rewrite Eq. (13) as

$$H_k = \sum_i \frac{\omega_i}{2}\left[-\frac{\partial^2}{\partial Q_i^2} - \left(\frac{\kappa_i^{(k)}}{\omega_i}\right)^2\right] + E_k + \sum_i \frac{\omega_i}{2}\left(Q_i + \frac{\kappa_i^{(k)}}{\omega_i}\right)^2, \quad (14)$$

where $\frac{\kappa_i^{(k)}}{\omega_i}$ is the normal coordinate difference between two electronic states, d_i, as denoted in Eq. (6). Therefore, the Huang-Rhys factors of five totally symmetric modes can be obtained.

For comparison, the gradients calculated in ref. [8] are reproduced in Table 2. Using these gradients, the corresponding Huang-Rhys factors are obtained and the results are also listed in Table 2. Apparently, the largest Huang-Rhys factor in the first excited state is from mode ν_{6a} (the value is about 0.837), which is in agreement with our results. The simulated absorption spectra of $S_1(^1B_{3u})$ state using the present theoretical framework and the four-mode model result (see Figure 9(b) in ref. [8]) are shown in Figure 3. Obviously, the present calculations reproduce the previous theoretical result reasonably, except the contribution of coupling mode $\nu_{10a;}$ in which the Huang-Rhys factor is zero.

4 Conclusions

In this work, the geometries and electronic structures of the ground and the first singlet excited state of pyrazine are detected in detail by using several quantum chemistry methods. The ground state geometries optimized by MP2 and CASSCF methods are quite reasonable compared with the experimental data[4] and the previous theoretical calculations[7,20]. As discussed in the previous

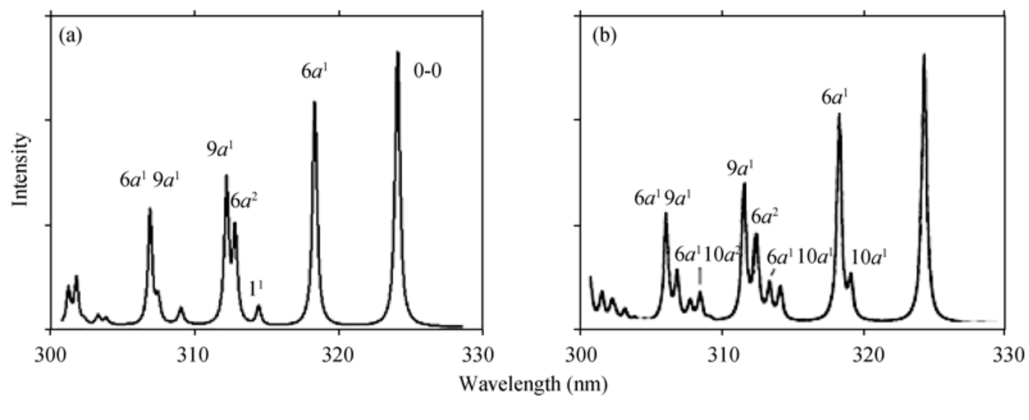

Figure 3 (a) The simulated absorption spectrum of $S_1(^1B_{3u})$ state using the *ab initio* data from ref. [8] within the present theoretical framework; (b) the four-orbital model result of ref. [8].

sections, the CIS and BHLYP geometries simulate unreasonable absorption spectrum profiles, which means that these two methods are unreliable for the geometrical optimization of the excited state in the present case. The electronic structure calculations confirm that the $S_1(^1B_{3u})$ state has nπ* configuration.

Using the Born-Oppenheimer approximation, the absorption spectra of $S_1(^1B_{3u})$ state of pyrazine are simulated by the conventional quantum mechanical method[18]. It is demonstrated that the distortion effect is unimportant for $S_1(^1B_{3u})$ absorption spectrum, except the coupling mode ν_{10a}. The calculated absorption spectra are in a reasonable agreement with experimental ones, which indicates that the present model without considering the conical intersection of S_1-S_2 can provide an acceptable interpretation. However, the vibronic line $10a^1$ induced by the mode ν_{10a} is not reproduced correctly, which denotes that the vibronic coupling between $S_2(^1B_{2u})$ and $S_1(^1B_{3u})$ state plays an important role in the $S_1(^1B_{3u})$ spectrum. Taking the *ab initio* data from ref. [8], the absorption spectrum of $S_1(^1B_{3u})$ state is reproduced within the present theoretical framework, and the result is in agreement with the theoretical spectrum excluding the effect of mode ν_{10a}.

1 Lahmani F, Ivanoff N. Mercury sensitization of the isomerization of diazines. J Phys Chem, 1972, 76: 2245－2248
2 Knight A E W, Parmenter C S. Radiative and nonradiative processes in the first excited singlet state of azabenzene vapors. Chem Phys, 1976, 15: 85－102
3 Yamazaki I, Murao T, Yamanaka T, Yoshihara K. Intramolecular electronic relaxation and photoisomerization processes in the isolated azabenzene molecules pyridine, pyrazine and pyrimidine. Faraday Discuss Chem Soc, 1983, 75: 395－405
4 Innes K K, Ross I G, Moonaw W R. Electronic states of azabenzenes and azanaphthalenes: A revised and extended critical review. J Mol Spectrosc, 1988, 132: 492－544
5 McDonald D B, Rice S A. Single vibronic level fluorescence from 1B3u pyrazine: The role of Fermi resonance and Duschinski rotation. J Chem Phys, 1981, 74: 4893－4906
6 Schneider R, Domcke W, KÖppel H. Aspects of dissipative electronic and vibrational dynamics of strongly vibronically coupled systems. J Chem Phys, 1990, 92: 1045－1061
7 Seidner L, Stock G, Sobolewski A L, Domcke W. *Ab initio* characterization of the S1–S2 conical intersection in pyrazine and calculation of spectra. J Chem Phys, 1992, 96: 5298－5309
8 Woywood C, Domcke W, Sobolewski A L, Werner H -J. Characterization of the S1–S2 conical intersection in pyrazine using *ab initio* multiconfiguration self-consistent-field and multireference configuration-interaction methods. J Chem Phys, 1994, 100: 1400－1413
9 Raab A, Worth G A, Meyer H -D, Cederbaum L S. Molecular dynamics of pyrazine after excitation to the S2 electronic state using a realistic 24-mode model Hamiltonian. J Chem Phys, 1999, 110: 936－946
10 Shalashilin D V, Child M S. Real time quantum propagation on a Monte Carlo trajectory guided grids of coupled coherent states: 26D simulation of pyrazine absorption spectrum. J Chem Phys, 2004, 121: 3563－3568
11 Wang L X, Meyer H -D, May V. Femtosecond laser pulse control of multidimensional vibrational dynamics: Computational studies on the pyrazine molecule. J Chem Phys, 2006, 125: 014102-1－014102-12
12 Stock G, Domcke W. Theory of resonance Raman scattering and fluorescence from strongly vibronically coupled excited states of polyatomic molecules. J Chem Phys, 1990, 93: 5496－5509
13 Child M S, Shalashilin D V. Locally coupled coherent states and Herman Kluk dynamics. J Chem Phys, 2003, 118: 2061－2071
14 Frisch M J, Trucks G W, Schlegel H B, Scuseria G E, Robb M A, Cheeseman J R, Montgomery J A, Jr., Vreven T, Kudin K N, Burant J C, Millam J M, Iyengar S S, Tomasi J, Barone V, Mennucci B, Cossi M, Scalmani G, Rega N, Petersson G A, Nakatsuji H, Hada M, Ehara M, Toyota K, Fukuda R, Hasegawa J, Ishida M, Nakajima T, Honda Y, Kitao O, Nakai H, Klene M, Li X, Knox J E, Hratchian H P, Cross J B, Bakken V, Adamo C, Jaramillo J, Gomperts R, Stratmann R E, Yazyev O, Austin A J, Cammi R, Pomelli C, Ochterski J W, Ayala P Y, Morokuma K, Voth G A, Salvador P, Dannenberg J J, Zakrzewski V G, Dapprich S, Daniels A D, Strain M C, Farkas O, Malick D K, Rabuck A D, Raghavachari K, Foresman J B, Ortiz J V, Cui Q, Baboul A G, Clifford S, Cioslowski J, Stefanov B B, Liu G, Liashenko A, Piskorz P, Komaromi I, Martin R L, Fox D J, Keith T, Al-Laham M A, Peng C Y, Nanayakkara A, Challacombe M, Gill P M W, Johnson B, Chen W, Wong M W, Gonzalez C, Pople J A. GAUSSIAN, Revision D02 (Gaussian, Inc., Wallingford CT, 2004)
15 Furche F, Ahlrichs R. Adiabatic time-dependent density functional methods for excited state properties. J Chem Phys, 2002, 117: 7433－7446
16 Ahlrichs R, Bär M, Häser M, Horn H, Kölmel C. Electronic structure calculations on workstation computers: The program system turbomole. Chem Phys Lett, 1989, 162: 165－169
17 Liang K K, Lin C K, Chang H C, Hayashi M, Lin S H. Theoretical treatments of ultrafast electron transfer from adsorbed dye molecule to semiconductor nanocrystalline surface. J Chem Phys, 2006, 125: 154706-1－154706-16
18 Lin S H, Bersohn R. Effect of radiation damping on dispersion. J Chem Phys, 1966, 44: 3768－3773
19 Hill T. An Introduction to Statistical Thermodynamics. Reading: Addison-Wesley Publ. Co.,1960. 89
20 Zhu L, Johnson P. Vibrations of pyrazine and its ion as studied by threshold ionization spectroscopy. J Chem Phys, 1993, 99: 2322－2331
21 Matsuzawa N N, Ishitani A, Dixon D A, Uda T. Time-dependent density functional theory calculations of photoabsorption spectra in the vacuum ultraviolet region. J Phys Chem A, 2001, 105: 4953
22 Li Y J, Wan J, Xu X. Theoretical study of the vertical excited states of benzene, pyrimidine, and pyrazine by the symmetry adapted cluster-configuration interaction method. J Comput Chem, 2007, 28: 1658－1667